Nano Research
DOI 10.1007/s12274-014-0471-6
Research Article
ISSN 1998-0124
CN 11-5974/O4

Piezotronic effect enhanced Schottky-contact ZnO micro/nanowire humidity sensor

Guofeng Hu[1,+], Ranran Zhou[1,+], Ruomeng Yu[2,+], Lin Dong[1], Caofeng Pan[1,*] (✉) and Zhong Lin Wang[1,2,*] (✉)

Nano Res., **Just Accepted Manuscript** • DOI: 10.1007/s12274-014-0471-6
http://www.thenanoresearch.com on March 30, 2014

Just Accepted

TABLE OF CONTENTS (TOC)

Piezotronic effect enhanced Schottky-contact ZnO micro/nanowire humidity sensor

Guofeng Hu[1,+], Ranran Zhou[1,+], Ruomeng Yu[2,+], Lin Dong[1], Caofeng Pan[1,*] (✉) and Zhong Lin Wang[1,2,*](✉)

1. Beijing Institute of Nanoenergy and Nanosystems, Chinese Academy of Sciences, Beijing, China, 100083

2. School of Materials Science and Engineering, Georgia Institute of Technology, Atlanta, Georgia, USA, 30332-0245

+ Authors contributed equally to this work.

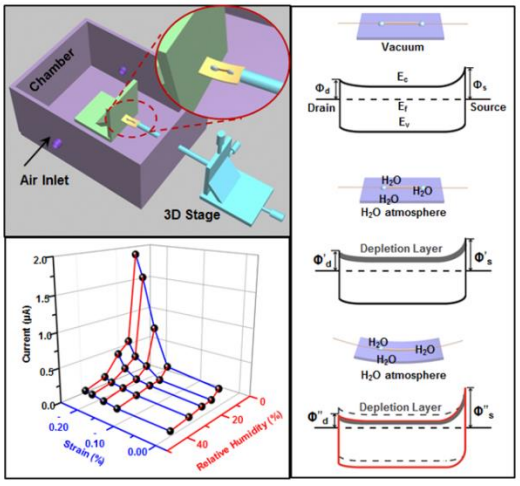

This work provides a new approach to profoundly improve the sensitivity and sensing resolution as well as highly enhance the signal level of Schottky-contact structured micro/nanowire sensing systems by piezotronic effect.

Caofeng Pan, http://124.16.153.201:8000/

Zhong Lin Wang, http://www.nanoscience.gatech.edu/

Nano Res.

DOI (automatically inserted by the publisher)
Research Article

Piezotronic effect enhanced Schottky-contact ZnO micro/nanowire humidity sensor

Guofeng Hu[1,+], Ranran Zhou[1,+], Ruomeng Yu[2,+], Lin Dong[1], Caofeng Pan[1,*] (✉) and Zhong Lin Wang[1,2,*] (✉)

1. Beijing Institute of Nanoenergy and Nanosystems, Chinese Academy of Sciences, Beijing, China, 100083
2. School of Materials Science and Engineering, Georgia Institute of Technology, Atlanta, Georgia, USA, 30332-0245
Address correspondence to: cfpan@binn.cas.cn, zlwang@gatech.edu
+ Authors contributed equally to this work.

ABSTRACT

A ZnO micro/nanowire was utilized to fabricate Schottky-contacted humidity sensors based on a metal-semiconductor-metal (M-S-M) structure. By introducing the piezotronic effect, the signal level, sensitivity and sensing resolution of the humidity sensor were largely enhanced by applying an external strain. Since a higher Schottky barrier largely reduces the signal level while a lower Schottky barrier decreases the sensor sensitivity due to increased ohmic transport, an optimum 0.22% compressive strain was determined to enhance the performances of the humidity sensor with the largest responsivity of 1,240%. The physical mechanism behind the observed mechanical-electrical behavior was carefully studied by using band structure diagram. This work provides a promising way to largely enhance the overall performance of a Schottky-contact structured micro/nanowire sensor.

KEYWORDS

Piezotronic effect, humidity sensor, ZnO micro/nanowire, Schottky contact

1 Introduction

Humidity monitoring is important in countless human's daily activities, including medicine[1], electronics[2], environmental monitoring[3], chemical processing[4], national defense[5] and scientific research[6]. Ever since the boosting age of nanoscience and nanotechnology, semiconducting nanowire based field effect transistors (FETs) have become one of the most promising candidates for various sensing systems due to their large surface to volume ratio as well as the flexibility and convenience of surface functionalization [7-9]. However, most of the conventional semiconducting micro/nanowire-based sensors take advantage of Ohmic contact in order to maximize the output signals. By changing the resistances of the device to realize sensing performances, Ohmic structured sensors require small size micro/nanowires in order to reduce the contact resistance as well as to improve the sensitivity, which makes them extremely difficult to be manipulated or fabricated[10]. Recently, much more easily fabricated micro/nanowire sensors utilizing Schottky-contact structure have been demonstrated to exhibit more enhanced sensitivity for detecting light, gases, and biomedical species[11-13]. Unlike Ohmic-contacted sensors, whose sensing performances highly depend on the changes of resistances, super-sensitive Schottky-contact sensors are achieved by tuning the Schottky Barrier Height (SBH) at local metal-semiconductor (M-S) interface, because a higher Schottky barrier largely reduces the signal level while a lower Schottky barrier decreases the sensor sensitivity due to increased ohmic transport [14-16]. Therefore, by finding a way to effectively control the barrier height at Schottky contact, one can ultimately reach the maximized performances of Schottky-contact sensors.

The piezotronic effect, usually existing in wurtzite/zinc blende family materials, has been proved and developed to be an effective way to tune/control the SBH at local M-S contact by applying an external strain on the whole structure[17-19]. The strain-induced polarization charges would produce a piezopotential distribution along the *c*-axis of micro/nanowire, which can increase or reduce the barrier height depending on the sign of the strains as well as the crystal's polar orientation[20,21]. It is demonstrated that the piezotronic effect can greatly improve the performance of nanowire-LEDs[22-24], photon detectors[25,26], FETs[27,28], NW solar cells[29], and photo-electrochemical devices[30]. In this work, we employed ZnO, one of the wurtzite family materials, as the building blocks to fabricate micro/nanowire sensors to monitor the relative humidity (RH) in ambient environment. By introducing the piezotronic effect, we successfully found a way to largely enhance the signal level, the sensitivity and the sensing resolution by introducing a static strain to the sensor. The physical mechanism behind the observed mechanical-electrical behavior was carefully

studied by using band structure diagram. This work provides a promising way to effectively enhance the overall performance of a Schottky-contact structured micro/nanowire sensor.

2 Experimental Sections

ZnO nanowires (NWs) were grown by a vapor-liquid-solid process at 960℃ (see Methods section for details), showing a hexagonal cross section with several hundred micrometers in lengths and hundreds of nanometers to several micrometers in diameters, as characterized by scanning electron microscopy (SEM) image presented in Fig. 1(a). Then, a long ZnO micro/nanowire was chosen and dispersed onto a polyethylene terephthalate (PET)/or a polystyrene (PS) substrate; both ends of the ZnO micro/nanowire were fixed by silver paste, serving as electrodes. After that a layer of epoxy was used to fully cover the two silver electrodes, preventing them from exposing in the air during the following test. An as-fabricated ZnO micro/nanowire humidity sensor was sealed in a humidity chamber with one end tightly fixed on the holder as schematically shown in Fig. 1(b). Piezotronic effect was introduced by bending the other end of the device through moving a positioner, which was attached to a 3D mechanical stage with movement resolution of 10 μm located outside the chamber, up and down to apply external strains. A typical digital image together with an optical microscopy image focusing on the micro/nanowire and metal electrodes of the device are presented in Fig. 1(c) and 1(d), respectively. The external strains applied to the device can be calculated according to Yang *et al.*'s work.

$$\varepsilon = h/2R,$$

where, ε is the strain of ZnO, h is the thickness of the substrate film, and R is the radius of the bending substrate, as shown in Fig. 1(e)[31].

3 Mechanism

A theoretical model is proposed to explain the piezotronic effect on the performances of ZnO micro/nanowire humidity sensors by utilizing energy band diagrams. Figure 1(f1) presents the energy band diagram of an M-S-M structured strain free ZnO micro/nanowire humidity sensor with its *c*-axis pointing from drain to source electrode. When introducing humid air into the chamber, water molecules were adsorbed onto the surface of ZnO micro/nanowire, where water dissociation occurred at surface oxygen vacancies (V_{Ox}) sites[32], leading to the formation of two bridging hydroxyl groups[33]. This process would reduce the carrier concentrations and form an electron depletion layer at the micro/nanowire surface, leading to a decrease of conductance of the whole device, as shown in Fig. 1(f2). The higher the RH, the lower the carrier density in ZnO micro/nanowire, and therefore the lower the output signals of the humidity sensor. If externally applying a compressive strain to the device at the same time, a strain-induced polarization

piezo-charges would occur at local M-S contacts at both ends with the *c*-axis pointing at the negative charge side owing to the non-central symmetric crystal structure of ZnO[21]. Such piezo-charges could be only partially screened instead of completely cancelled out since they are non-mobile ionic charges[34], although hydronium (H_3O^+) would be dissociated by water molecules to produce hydroxyl ion (OH^-) in a moisture environment,[35-37], and thus lead to a directional movement of free electrons towards the piezo-charges in a moisture environment. As a result, the SBH at drain electrode, Φ_d, was reduced due to the presence of positive piezo-charges, while the SBH at source electrode was increased on the other end as shown in Fig. 1(f3).

For a reversely biased SB contact, the carriers transport process is dominated by the local SBH Φ_d, following an exponential way[38,39], that is to say, a tiny change of the local SBH Φ_d, would lead to a great change of the current through the Schottky contact. The *piezotronic effect* is right to use piezo-charges to tune/control the charge transport across an interface/junction[40]. As a result, the decrease of the local SBH Φ_d, when increased the externally applied compressive strain, led to a higher output signal and sensitivity of the ZnO micro/nano humidity sensors.

4 Results and discussion

Systematic measurements of humidity sensors were conducted under different RH and strain conditions at room temperature. For a strain free and a -0.20% compressively strain ZnO micro/nanowire humidity sensor, typical *I-V* characteristics under different RHs are presented in Figs. 2(a) and 2(b), respectively. The derived non-linear and non-symmetrical *I-V* curves indicate that the barrier heights at two Schottky contacts are distinguishable (Fig. 1(f)). As predicted by the working principles described above (Fig. 1(f2)), the output signals (i.e. current) decreased when increasing the RH in a monotonous manner for both cases, a clear trend can be observed by extracting current value at fixed 2.8 V with drain electrode reversely biased as presented at most right side of Fig. 2(a) and 2(b) correspondingly. Under 0.00% strain (Fig. 2(a)), the current decreased from 365.0 nA to 8.72 nA when the RH increased from ~15.0% to ~66.0%, while the current decreased from 884 nA to 12.9 nA as shown in Fig. 2(b), when the humidity sensor was -0.22% compressively strained, which indicates that the piezotronic effect could largely enhance the resolution of the humidity sensor, which could be considered as $\Delta I/\Delta RH$.

These I-V characteristics clearly demonstrate that there were Schottky barriers presenting at the two ZnO/Ag contacts but with distinctly different barrier heights. These Schottky barriers at the metal/semiconductor interfaces play a crucial role in determining the electrical transport property of the M-S-M structure. For a better understanding of the behavior of this humidity sensor, an equivalent

circuit model (inset of Fig. 2(c)) is built for the case of Fig. 2(a), and the fitting of the I-V characteristics of the devices was carried out using a GUI program PKUMSM developed by Peng et al[41]. The fitting results are plotted as a red line in Fig. 2(c), together with the experimental data in blue dots. Furthermore, the changes of SBH at both ends, Φ_d and Φ_s, as well as the resistance of a strain free ZnO micro/nanowire humidity sensor are also calculated under different RHs as presented in Figs. 2(d) and 2(e). Apparently, the SBHs changed randomly with the RHs, while the resistance increased with the increasing of RHs, which can be accounted for the decrease of output signal observed in Figs. 2(a) and (b). This behavior is consisted with the mechanism described above very well, since the intrinsic defect VO_x in ZnO, has a level below the conduction band and plays an important role in the conductivity of ZnO. When ZnO micro/nanowire was exposed to humid air, water molecules were adsorbed onto the surface of ZnO micro/nanowire and formed hydroxyl species, water monolayer, or even water film with the incensement of humidity[42], reducing the carrier concentrations and forms an electron depletion layer at the micro/nanowire surface, finally decreases the conductivity of ZnO micro/nanowire. Piezotronic effect on ZnO micro/nanowire humidity sensors was explored by applying different strains under certain RHs. Figures 3(a) and 3(b) show the typical *I-V* characteristics together with the extracted current changes under a fixed 2.8 V bias voltage (drain electrode reversely biased) for two typical humidities RH 25.5% and 32.9%, respectively. It can be seen the output signal increases monotonously with increasing the externally applied compressive strains at a fixed RH as indicated by the working principle of ZnO micro/nanowire humidity sensors when drain electrode was reversely biased. Theoretical simulations were also conducted to derive the changes of SBH at both ends (Fig. 3(b) and 3(d)), showing that Φ_d decreased with increasing the compressive strains in both RH cases.

A 3-dimensional (3D) scatter plot is presented in Fig. 4(a) to show the humidity sensor's performances at a fixed bias of 2.8 V under different humidity and strain conditions. The overall trend of output signals changes can be concluded straightforwardly by correlating it with RH and compressive strains. The current monotonously increases with the increment of compressive strain, while decreases with the increment of RH. Two 2D graphs are extracted from Fig. 4(a) to display the outputs response to different compressive strains and RHs under certain circumstances as shown in Fig. 4(b) and 4(c), respectively. As a 2D projection of the 3D plot in Fig. 4(a) on *I-strain* surface, five curves immersed in five different RHs were derived by measuring the output current of the ZnO humidity sensor under different compressive strains in each case, as shown in Fig. 4(b). Overall, the current decreased with increasing the RH due to the adsorption of

water molecules as explained above. For each curve, the output signals increased with the increasing compressive strains, confirming that the piezotronic effect can enhance the general performances of humidity sensors at different RH by rising up the signal levels. Moreover, by looking into the current differences between two certain RHs under different strain conditions in Fig. 4(b), it can be concluded that such differences were significantly enlarged by applying more compressive strains, which indicates a huge improvement of the sensing resolution of ZnO micro/nanowire humidity sensors by piezotronic effect. For example, the current increased from 0.15 μA (~RH 15.0%) to 0.25 μA (~RH 19.6%) under no strain, where a 66.7% relative change in current was obtained; while this same current difference appeared to be from 0.64 μA (15.0% RH) to 1.92 μA (~RH 19.6%) under -0.22% compressive strain, with a 200% relative change in current achieved. These results clearly show a significant enhancement of the sensing resolution of our humidity sensors by piezotronic effect. A similar conclusion can be obtained by projecting the same 3D plot on *I-RH* surface as presented in Fig. 4(c). Moreover, the slope of curves became deeper and deeper when the applied strain increased, which means the sensitivity of humidity sensors was improved by the piezotronic effect as well.

To optimize the performances of the ZnO micro/nanowire humidity sensor, the relative changes of output current with respect to changing compressive strains and RHs are plotted as another two 3D scatter graphs in Figs. 4(d) and 4(f), from which two 2D graphs are extracted to provide more details and information as shown in Figs. 4(e) and 4(g). By looking into the relative current response to various RHs under each certain strain condition as shown in Figs. 4(d) and 4(e), it is obvious to conclude that the larger the compressive strain, the larger the relative changes can be obtained from output signals. Therefore, a -0.22% compressive strain in our case can optimize the performances of ZnO micro/nanowire humidity sensor by achieving a largest responsivity of 1,240%.

Finally, the stability of ZnO micro/nanowire sensor in humid air was testified in our experiments. During the experiments, the device was strained in a chamber with fixed humidity, and it was tested for several hours to obtained a group of data, and then it was left to dry for one hour followed by measurements for another several hours. This process was repeated for seven times at seven different humidities. Typically, it took several days to finish the whole procedure of measuring one device. Our results show that the devices can perform stably during a series of experiments. Therefore, ZnO micro/nanowires can maintain their stability in the humid air for a time period long enough for repeated measurements thousands of times in practical applications, and the ZnO micro/nanowires device was reported very stable as a glucose sensor even in a aqueous solution.[14]

5 Conclusions

In summary, an M-S-M structured Schottky-contacted ZnO micro/nanowire device was presented to work as a humidity sensor. The piezotronic effect on the ZnO micro/nanowire humidity sensor can not only highly enhance the signal level, but also significantly improve its sensitivity and sensing resolution. A -0.22% compressive strain was determined to optimize the performances of humidity sensor with the largest responsivity of 1240% achieved among a series of the relative humidities. A physical mechanism was carefully studied to explain the observed mechanical-electrical behavior of this humidity sensor by using band structure diagram. This work provides a new approach to profoundly improve the sensitivity and sensing resolution as well as highly enhance the signal level of Schottky-contact structured micro/nanowire sensing systems.

Acknowledgements

The authors thank for the support from the "thousands talents" program for pioneer researcher and his innovation team, China; the Knowledge Innovation Program of the Chinese Academy of Sciences，Grant No. KJCX2-YW-M13); and the president funding, Chinese Academy of Sciences.

Methods

ZnO micro/nanowire synthesis and characterization. ZnO micro/nanowires were synthesized via the vapor-liquid-solid growth process [43-45]. An alumina boat loaded with 0.5 g ZnO and 0.5 g carbon mixture powders were placed in the center of the tube furnace, while the silicon substrate coated with 5 nm Au was horizontally mounted on top of the boat with the Au layer facing down. The typical synthesis procedure was carried out at a temperature of 960℃ with the flow rate of Argon gas at 100 sccm for 1 h.

Device fabrication. The ZnO device was fabricated by transferring and bonding an individual ZnO micro/nanowire laterally onto a flexible polystyrene (PS) substrate, with its *c*-axis in the plane of the substrate pointing from drain to source electrode. Silver paste was applied to fix both ends of the micro/nanowire and also serve as source and drain electrodes.

Measurement and piezotronic effect on a ZnO humidity sensor. One end of the as-fabricated device was tightly fixed on a holder sealed inside a constant temperature chamber. A positioner which could be controlled from outside of the chamber with a 3D mechanical stage was utilized to bend the free end of the device to introduce compressive strains. Humid air was introduced into the chamber through an air inlet, as shown in Fig. 1(b), with a hygrometer continuously monitoring the

RH inside the chamber to maintain it at a constant level. The performances of the device under different strains were measured using a computer-controlled measurement system.

References

[1] Borini, S.;White, R.;Wei, D.;Astley, M.;Haque, S.;Spigone, E.;Harris, N.;Kivioja, J.; Ryhänen, T. Ultrafast Graphene Oxide Humidity Sensors. *ACS Nano* **2013**, *7*, 11166-11173.

[2] Saeidi, N.;Strutwolf, J.;Marechal, A.;Demosthenous, A.; Donaldson, N. A Capacitive Humidity Sensor Suitable for CMOS Integration. *IEEE Sens. J* **2013**, *13*, 4487-4495.

[3] Amin, E.;Bhuiyan, M.;Karmakar, N.; Winther-Jensen, B. Development of a Low Cost Printable Chipless RFID Humidity Sensor. *IEEE Sens. J* **2014**, *14*, 140-149.

[4] Wang, X.;Zhao, C.-L.;Li, J.;Jin, Y.;Ye, M.; Jin, S. Multiplexing of PVA-coated multimode-fiber taper humidity sensors. *Opt. Commun.* **2013**, *308*, 11-14.

[5] Hsueh, H.-T.;Chen, Y.-H.;Lin, Y.-D.;Lai, K.-C.;Chen, J.-W.; Wu, C.-L. Integration of flower-like ZnO nanostructures with crystalline-Si interdigitated back contact photovoltaic cell as a self-powered humidity sensor. *Appl. Phys. Lett.* **2013**, *103*, 213109.

[6] Tahir, M.;Sayyad, M. H.;Clark, J.;Wahab, F.;Aziz, F.;Shahid, M.;Munawar, M. A.; Chaudry, J. A. Humidity, light and temperature dependent characteristics of Au/N-BuHHPDI/Au surface type multifunctional sensor. *Sens. Actuators B: Chem.* **2014**, *192*, 565-571.

[7] Cui, Y.; Lieber, C. M. Functional nanoscale electronic devices assembled using silicon nanowire building blocks. *Science* **2001**, *291*, 851-853.

[8] Duan, X.;Huang, Y.;Cui, Y.;Wang, J.; Lieber, C. M. Indium phosphide nanowires as building blocks for nanoscale electronic and optoelectronic devices. *Nature* **2001**, *409*, 66-69.

[9] Arnold, M. S.;Avouris, P.;Pan, Z. W.; Wang, Z. L. Field-effect transistors based on single semiconducting oxide nanobelts. *J. Phys. Chem. B* **2003**, *107*, 659-663.

[10] Kuang, Q.;Lao, C.;Wang, Z. L.;Xie, Z.; Zheng, L. High-sensitivity humidity sensor based on a single SnO_2 nanowire. *J. Am. Chem. Soc.* **2007**, *129*, 6070-6071.

[11] Wei, T.-Y.;Yeh, P.-H.;Lu, S.-Y.; Wang, Z. L. Gigantic enhancement in sensitivity using Schottky contacted nanowire nanosensor. *J. Am. Chem. Soc.* **2009**, *131*, 17690-17695.

[12] Zhou, J.;Gu, Y.;Hu, Y.;Mai, W.;Yeh, P.-H.;Bao, G.;Sood, A. K.;Polla, D. L.; Wang, Z. L. Gigantic enhancement in response and reset time of ZnO UV nanosensor by utilizing Schottky contact and surface functionalization. *Appl. Phys. Lett.* **2009**, *94*, 191103.

[13] Yeh, P. H.;Li, Z.; Wang, Z. L. Schottky-Gated Probe-Free ZnO Nanowire Biosensor. *Adv. Mater.* **2009**, *21*, 4975-4978.

[14] Yu, R.;Pan, C.;Chen, J.;Zhu, G.; Wang, Z. L. Enhanced Performance of a ZnO Nanowire-Based Self‐Powered Glucose Sensor by Piezotronic Effect. *Adv. Funct. Mater.* **2013**, *23*, 5868-5874.

[15] Yu, R.;Pan, C.; Wang, Z. L. High performance of ZnO nanowire protein sensors enhanced by the piezotronic effect. *Energ. Environ. Sci.* **2013**, *6*, 494-499.

[16] Pan, C.;Yu, R.;Niu, S.;Zhu, G.; Wang, Z. L. Piezotronic Effect on the Sensitivity and Signal Level of Schottky Contacted Proactive Micro/Nanowire Nanosensors. *ACS Nano* **2013**, *7*, 1803-1810.

[17] Zhang, Y.;Liu, Y.; Wang, Z. L. Fundamental theory of piezotronics. *Adv. Mater.* **2011**, *23*, 3004-3013.

[18] Wang, Z. L. Piezopotential gated nanowire devices: Piezotronics and piezo-phototronics. *Nano Today* **2010**, *5*, 540-552.

[19] Wu, W.;Pan, C.;Zhang, Y.;Wen, X.; Wang, Z. L. Piezotronics and piezo-phototronics–From single nanodevices to array of devices and then to integrated functional system. *Nano Today* **2013**, *8*, 619-642.

[20] Gao, Y.; Wang, Z. L. Electrostatic potential in a bent piezoelectric nanowire. The fundamental theory of nanogenerator and nanopiezotronics. *Nano Lett.* **2007**, *7*, 2499-2505.

[21] Wang, Z. L. Piezotronic and piezophototronic effects. *J. Phys. Chem. Lett.* **2010**, *1*, 1388-1393.

[22] Yang, Q.;Liu, Y.;Pan, C. F.;Chen, J.;Wen, X. N.; Wang, Z. L. Largely Enhanced Efficiency in ZnO Nanowire/p-Polymer Hybridized Inorganic/Organic Ultraviolet Light-Emitting Diode by Piezo-Phototronic Effect. *Nano Lett.* **2013**, *13*, 607-613.

[23] Pan, C. F.;Dong, L.;Zhu, G.;Niu, S. M.;Yu, R. M.;Yang, Q.;Liu, Y.; Wang, Z. L. High-resolution electroluminescent imaging of pressure distribution using a piezoelectric nanowire LED array. *Nat. Photon.* **2013**, *7*, 752-758.

[24] Yang, Q.;Wu, Y. P.;Liu, Y.;Pan, C. F.; Wang, Z. L. Features of the piezo-phototronic effect on optoelectronic devices based on wurtzite semiconductor nanowires. *PCCP* **2014**, *16*, 2790-2800.

[25] Liu, Y.;Yang, Q.;Zhang, Y.;Yang, Z. Y.; Wang, Z. L. Nanowire Piezo-phototronic Photodetector: Theory and Experimental Design. *Adv. Mater.* **2012**, *24*, 1410-1417.

[26] Dong, L.;Niu, S. M.;Pan, C. F.;Yu, R. M.;Zhang, Y.; Wang, Z. L. Piezo-Phototronic Effect of CdSe Nanowires. *Adv. Mater.* **2012**, *24*, 5470-5475.

[27] Liu, W. H.;Lee, M.;Ding, L.;Liu, J.; Wang, Z. L. Piezopotential Gated Nanowire-Nanotube Hybrid Field-Effect Transistor. *Nano Lett.* **2010**, *10*, 3084-3089.

[28] Zhou, Y. S.;Wang, K.;Han, W. H.;Rai, S. C.;Zhang, Y.;Ding, Y.;Pan, C. F.;Zhang, F.;Zhou, W. L.; Wang, Z. L. Vertically Aligned CdSe Nanowire Arrays for Energy Harvesting and Piezotronic Devices. *ACS Nano* **2012**, *6*, 6478-6482.

[29] Pan, C. F.;Niu, S. M.;Ding, Y.;Dong, L.;Yu, R. M.;Liu, Y.;Zhu, G.; Wang, Z. L. Enhanced Cu_2S/CdS Coaxial Nanowire Solar Cells by Piezo-Phototronic Effect. *Nano Lett.* **2012**, *12*, 3302-3307.

[30] Starr, M. B.;Shi, J.; Wang, X. D. Piezopotential-Driven Redox Reactions at the Surface of Piezoelectric Materials. *Angew. Chem. Int. Edit.* **2012**, *51*, 5962-5966.

[31] Yang, R.;Qin, Y.;Dai, L.; Wang, Z. L. Power generation with laterally packaged piezoelectric fine wires. *Nat. Nanotechnol.* **2009**, *4*, 34-39.

[32] Janotti, A.; Van de Walle, C. G. Oxygen vacancies in ZnO. *Appl. Phys. Lett.* **2005**, *87*, 122102.

[33] Schaub, R.;Thostrup, P.;Lopez, N.;Lægsgaard, E.;Stensgaard, I.;Nørskov, J. K.; Besenbacher, F. Oxygen Vacancies as Active Sites for Water Dissociation on Rutile TiO_ {2}(110). *Phys. Rev. Lett.* **2001**, *87*, 266104.

[34] Zhou, J.;Fei, P.;Gu, Y.;Mai, W.;Gao, Y.;Yang, R.;Bao, G.; Wang, Z. L. Piezoelectric-potential-controlled polarity-reversible Schottky diodes and switches of ZnO wires. *Nano Lett.* **2008**, *8*, 3973-3977.

[35] Geissler, P. L.;Dellago, C.;Chandler, D.;Hutter, J.; Parrinello, M. Autoionization in liquid water. *Science* **2001**, *291*, 2121-2124.

[36] Dulub, O.;Meyer, B.; Diebold, U. Observation of the dynamical change in a water monolayer adsorbed on a ZnO surface. *Phys. Rev. Lett.* **2005**, *95*, 136101.

[37] Du, Y.;Deskins, N. A.;Zhang, Z.;Dohnalek, Z.;Dupuis, M.; Lyubinetsky, I. Two Pathways for Water Interaction with Oxygen Adatoms on TiO_2(110). *Phys. Rev. Lett.* **2009**, *102*.

[38] Yu, R. M.;Dong, L.;Pan, C. F.;Niu, S. M.;Liu, H. F.;Liu, W.;Chua, S.;Chi, D. Z.; Wang, Z. L. Piezotronic Effect on the Transport Properties of GaN Nanobelts for Active Flexible Electronics. *Adv. Mater.* **2012**, *24*, 3532-3537.

[39] Sze, S. M. *Physics of semiconductor deVices*; John Wiley & Sons: New Yorks, 1981.

[40] Wang, Z. L. Nanopiezotronics. *Adv. Mater.* **2007**, *19*, 889-892.

[41] Liu, Y.;Zhang, Z. Y.;Hu, Y. F.;Jin, C. H.; Peng, L. M. Quantitative Fitting of Nonlinear Current–Voltage Curves and Parameter Retrieval of Semiconducting Nanowire, Nanotube and Nanoribbon Devices. *J Nanosci. Nanotechnol.* **2008**, *8*, 252-258.

[42] Hu, H.;Ji, H.-F.; Sun, Y. The effect of oxygen vacancies on water wettability of a ZnO surface. *PCCP* **2013**, *15*, 16557-16565.

[43] Wang, X.;Wang, X.;Summers, C. J.; Wang, Z. L. Large-scale hexagonal-patterned growth of aligned ZnO nanorods for nano-optoelectronics and nanosensor arrays. *Nano Lett.* **2004**, *4*, 423-426.

[44] Pan, C. F.; Zhu, J. The syntheses, properties and applications of Si, ZnO, metal, and heterojunction nanowires. *J. Mater. Chem.* **2009**, *19*, 869-884.

[45] Zhu, G.;Zhou, Y.;Wang, S.;Yang, R.;Ding, Y.;Wang, X.;Bando, Y.; lin Wang, Z. Synthesis of vertically aligned ultra-long ZnO nanowires on heterogeneous substrates with catalyst at the root. *Nanotechnology* **2012**, *23*, 055604.

Figures and figure captions

Figure 1

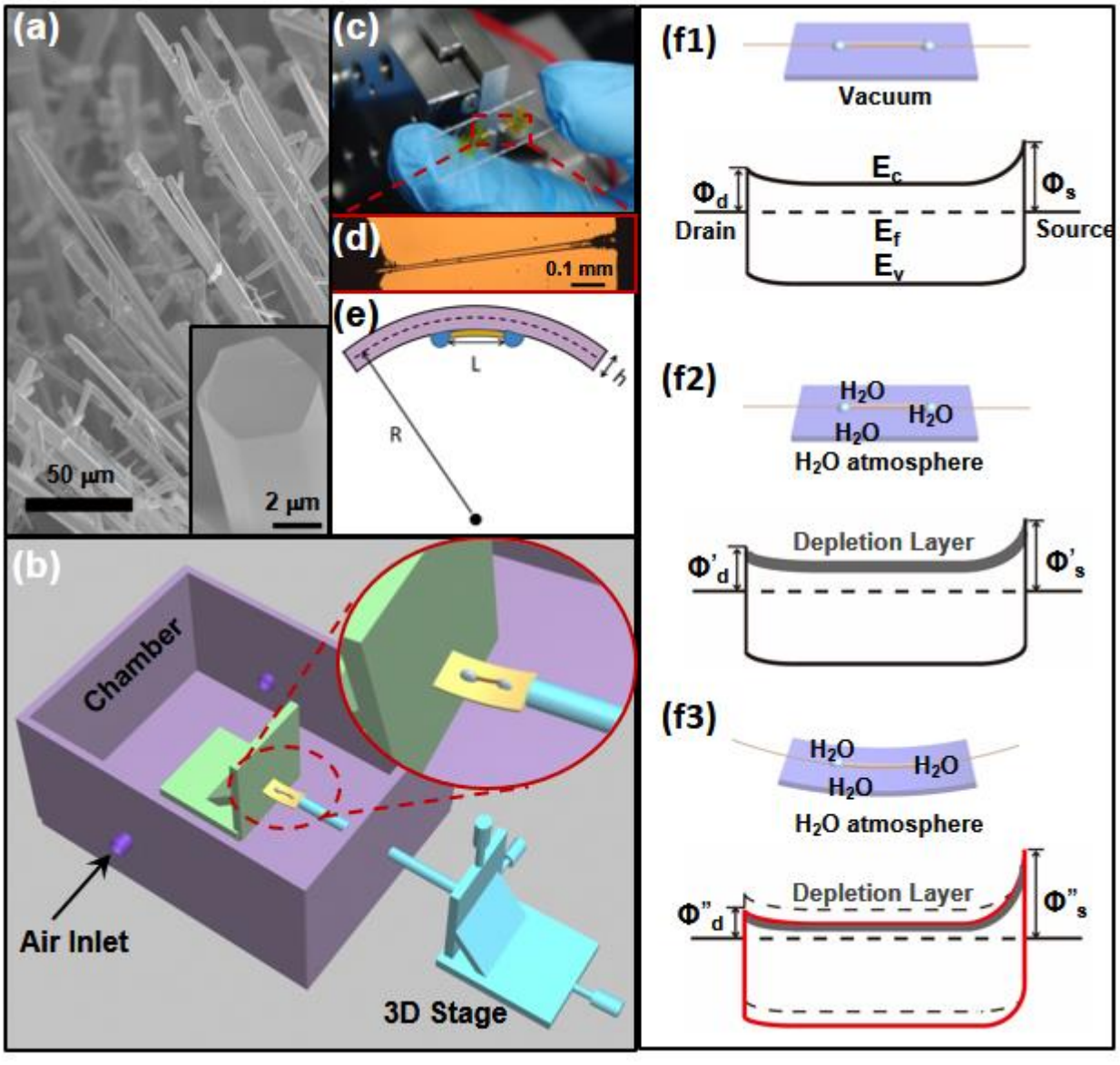

Figure 1 (a) Scanning electron microscopy (SEM) image of the as-grown ZnO NWs; Inset: enlarged SEM image of an individual ZnO NW, showing a perfect hexagonal cross-section. (b) Schematic of the measurement setups. (c) The optical image of an as-fabricated humidity sensor; (d) The optical microscopy image of the as-fabricated device. (e) Schematic shows the calculation of the compressive strain applied to the device. (f) Schematic energy band diagrams of ZnO NW humidity sensors, (f1) vacuum, (f2) H2O atmosphere, (f3) compressively strain in H2O atmosphere.

Figure 2

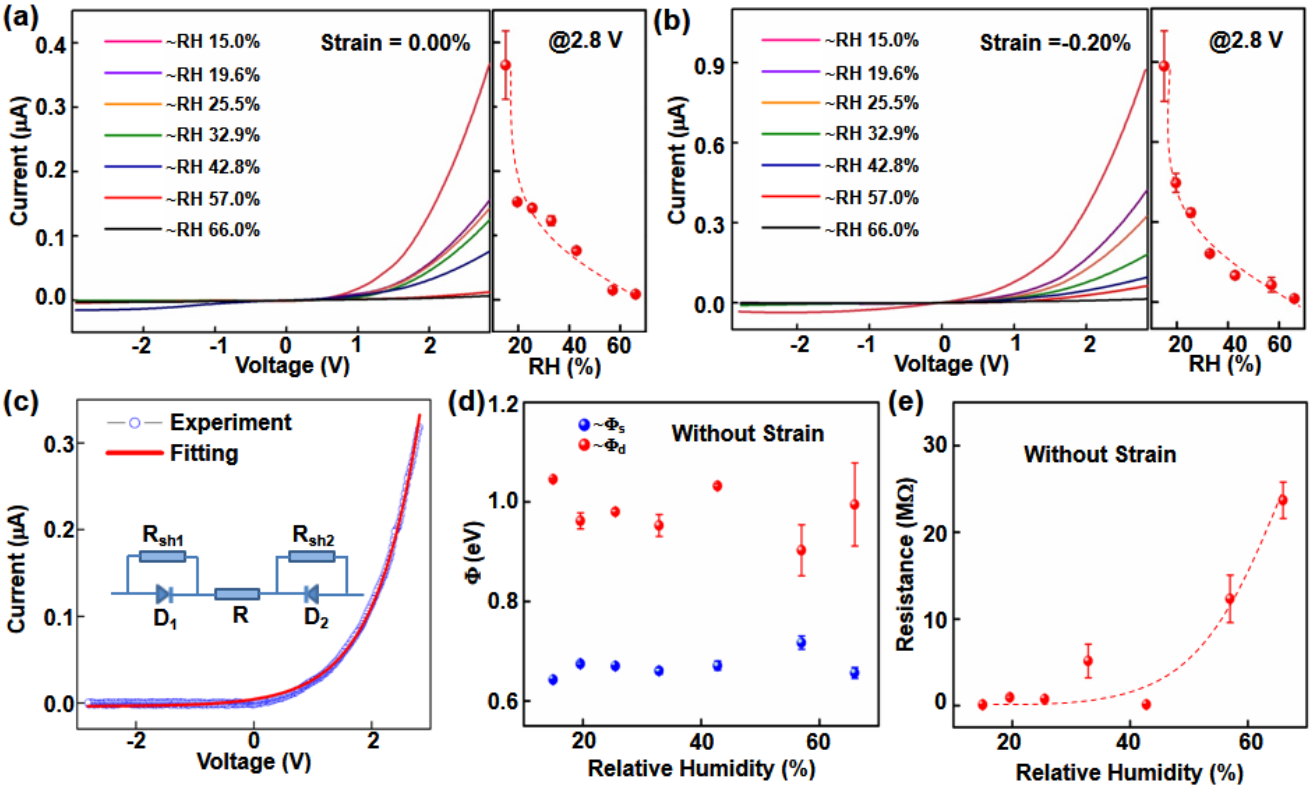

Figure 2 (a-b) I-V curves of the humidity sensor at different RHs, the compressive strain was 0.00% (a) and 0.20% (b) respectively. (c) Equivalent circuit model and quantitative fitting result of an individual ZnO NW-based humidity sensor. (d) The fitting results of the two Schottky barrier height changes with RHs from 15% to 66% without strain. (e) The fitting results of the resistance of the device with RHs from 15% to 66% without strain.

Figure 3

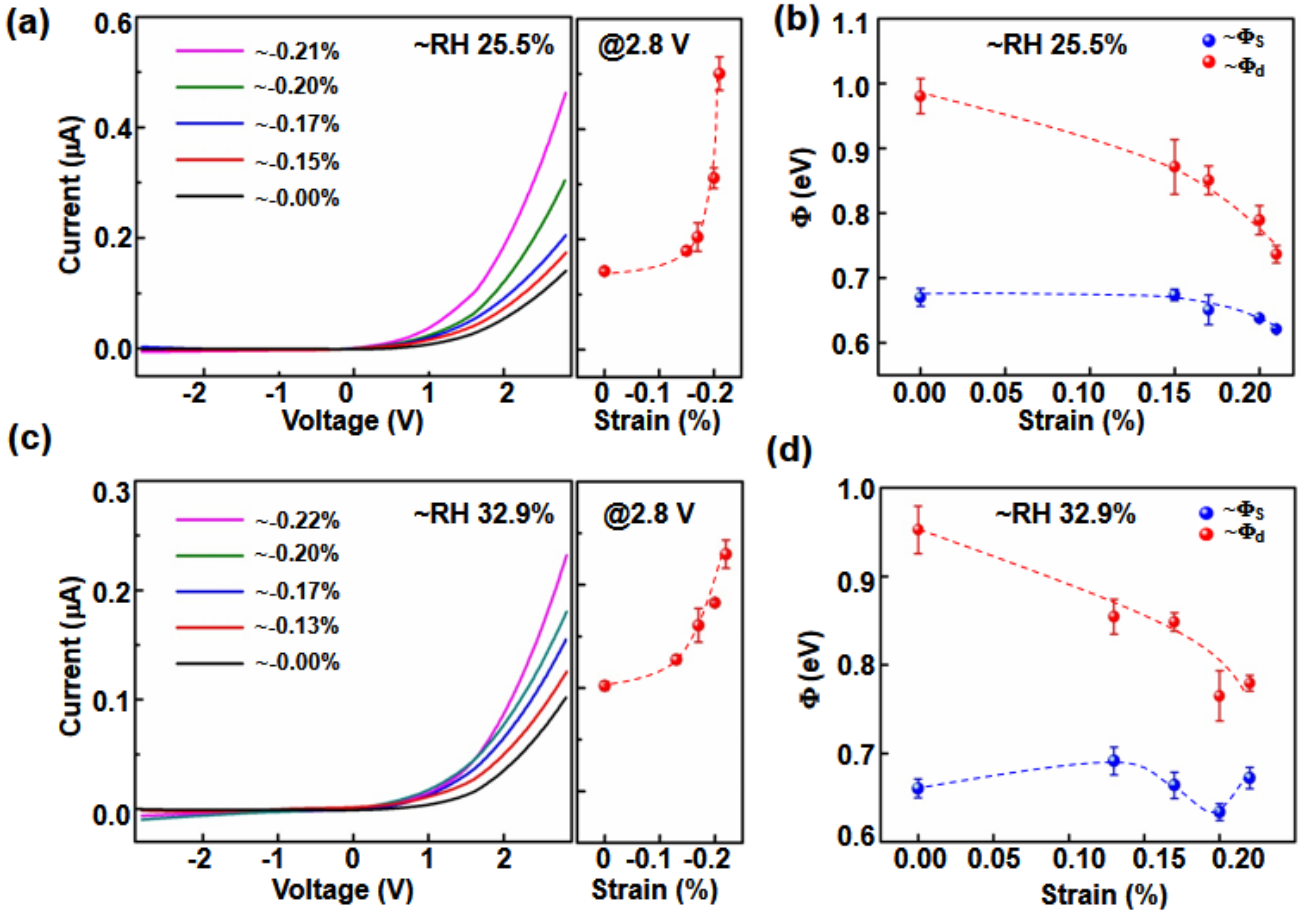

Figure 3 (a)&(c) I-V curves of the humidity sensor at different compressive strains, the RH was 25.5% (a) and 32.9% (c), respectively. (b)&(d) The fitting results of the two Schottky barrier height changes with compressive strains from 0 to 0.22%, the RH was 25.5% and 32.9% respectively.

Figure 4

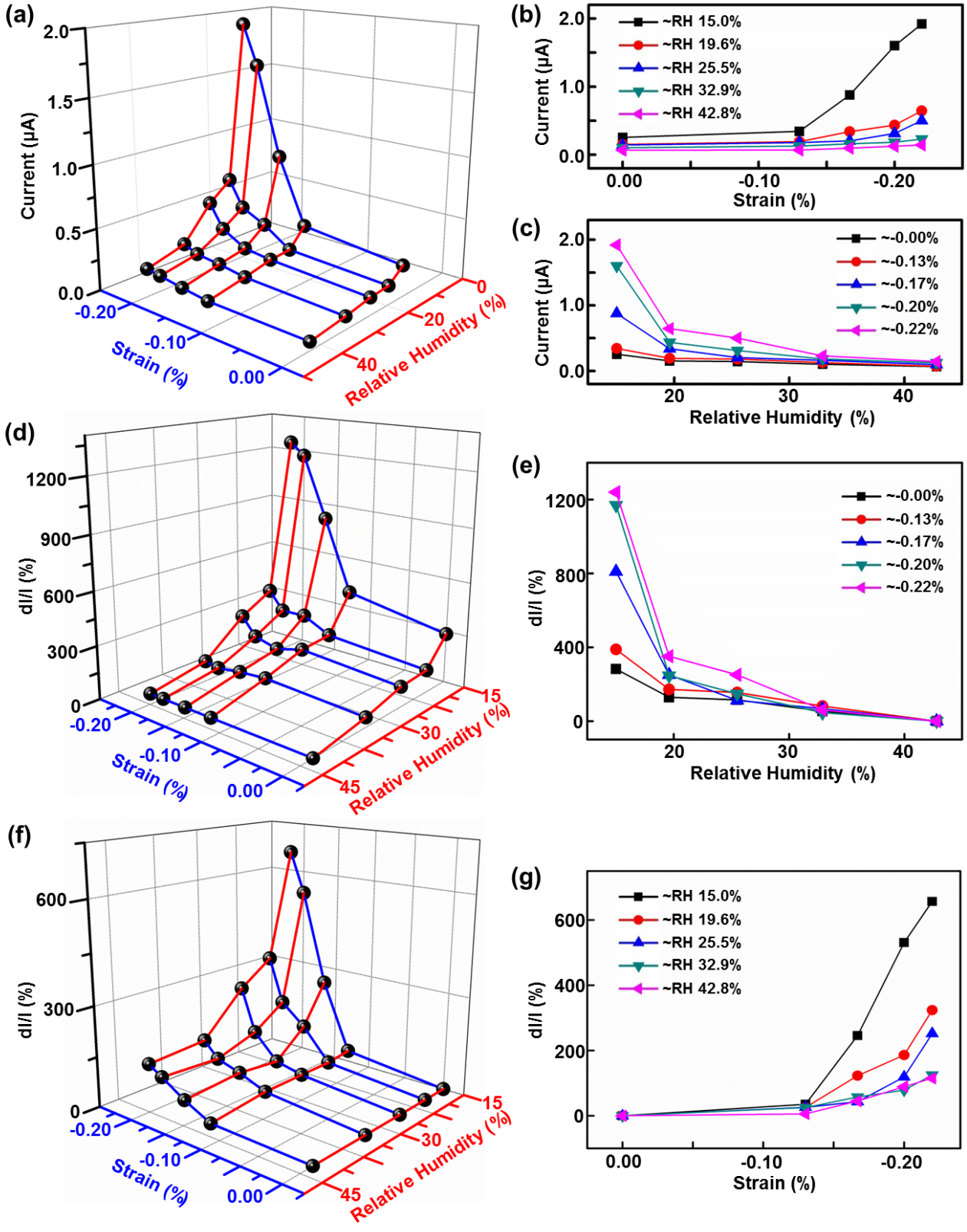
(a)
Current (μA)
Strain (%)
Relative Humidity (%)
(b)
~RH 15.0%
~RH 19.6%
~RH 25.5%
~RH 32.9%
~RH 42.8%
Current (μA)
Strain (%)
(c)
~-0.00%
~-0.13%
~-0.17%
~-0.20%
~-0.22%
Current (μA)
Relative Humidity (%)
(d)
dI/I (%)
Strain (%)
Relative Humidity (%)
(e)
~-0.00%
~-0.13%
~-0.17%
~-0.20%
~-0.22%
dI/I (%)
Relative Humidity (%)
(f)
dI/I (%)
Strain (%)
Relative Humidity (%)
(g)
~RH 15.0%
~RH 19.6%
~RH 25.5%
~RH 32.9%
~RH 42.8%
dI/I (%)
Strain (%)

Figure 4 (a) 3D graph depicting the current response of the ZnO NW humidity sensor to strain and relative humidity at a bias voltage equal to 2.8 V. (b) Absolute current response to different compressive strains, with relative humidity ranging from 15.0% to 42.8%. (c) Absolute current response to different relative humidities, with compressive strains ranging from -0.00%to -0.22%. (d) 3D graph and its corresponding 2D projection (e) indicate the relative changes of current with respect to the value at 42.8% RH, under different compressive strains ranging from -0.00% to -0.22%. (f) 3D graph and its corresponding 2D projection (g) indicate the relative changes of current with respect to the value at 0.0% strain, under different RHs ranging from 15.0% to 42.8%.